Automated road pavement marking detection from high resolution aerial images based on Multi-resolution image analysis and anisotropic Gaussian filtering

Hang Jin
Faculty of Science and Technology
Queensland University of Technology
Brisbane, Australia
E-mail: jinhang3695@gmail.com

Yanming Feng
Faculty of Science and Technology
Queensland University of Technology
Brisbane, Australia
E-mail: y.feng@qut.edu.au

***Abstract*—Road features extraction from remote sensed imagery has been a long-term topic of great interest within the photogrammetry and remote sensing communities for over three decades. The majority of the early work only focused on linear feature detection approaches, with restrictive assumption on image resolution and road appearance. The widely available of high resolution digital aerial images makes it possible to extract sub-road features, e.g. road pavement markings. In this paper, we will focus on the automatic extraction of road lane markings, which are required by various lane-based vehicle applications, such as, autonomous vehicle navigation, and lane departure warning. The proposed approach consists of three phases: i) road centerline extraction from low resolution image, ii) road surface detection in the original image, and iii) pavement marking extraction on the generated road surface. The proposed method was tested on the aerial imagery dataset of the Bruce Highway, Queensland, and the results demonstrate the efficiency of our approach.**

Keywords-road pavement marking; feature extraction; high resolution aerial image; multi-resolution image analysis; anosotropic Gaussian filtering

I. INTRODUCTION

Nowadays there is a growing need for accurate road models for various applications e.g. traffic monitoring, city planning and autonomous navigation. Especially the advanced vehicle assistance system (ADAS), includes applications such as lane departure warning, lane-level vehicle navigation, asks for not only the directional information but also the accurate road lane marking details, for example, the number of lanes, the location and type of lane markings.

Vehicle-based mobile mapping system (MMS) is a widely used method for detailed road information acquisition. Many research studies of detection and reconstruction of road marks have been carried out in the field of terrestrial imagery or close range photogrammetry. Due to the difference in data acquisition platform, input data, type of feature fused for road identification, approaches developed for road geometry extraction based on MMS are quite different from each other. For instance, lane markings are extracted based on thresholding [1], frequency analysis [2]; or from structures, such as linear or curve [3], Snake [4]; or even image classification [5]. An exhaustive review of road marking reconstruction approaches based on ground photogrammetry can be referred to [6]. However, the drawback of MMS is also apparent: it is costly and time-consuming, which is not suitable for date collection in large areas.

Another method for road lane marking acquisition is through feature extraction from remote sensed images. However, due to the limitation of the ground resolution of images, most of the existing approaches only concentrate on the detection of road centerline rather than other sub-surface details. Only a few approaches involved the detection of lane markings in the extraction of road centerlines. For example, Steger et al. [7] extract the collinear road markings as bright objects in large scale photographs when the roadsides exhibit no visible edges. Hinz and Baumgartner [8] utilized road mark features, detected as thin bright lines with symmetric contrast, as the evidence for the presence of a road. Besides, an automatic vehicle detection module is also employed to eliminate the gap of lane segments caused by cars. Another approach of road extraction with pavement markings detection is presented in [9], where the road marks and zebra crossing are segmented based on coloristic and geometric characteristics. The detected road marks and zebra crossing are then used as clues for the local direction and width of the road. The similar work can also been found in [10], where the road mark portions are extracted primarily based on radiometry variation to provide topology and geometry support. On the whole, road pavement marks are only regarded as a clue to reconstruct the road network, and thus not being focused in. Therefore, the quality requirements [11], such as robustness, quality, completeness, are far below the lane level applications.

In more recent works, Kim et al. [12] built a system specially designed to extract pavement information for car navigation. Tournaire et al. [11] proposed a specific approach for dashed lines and zebra crossing reconstruction, which relied on external knowledge introduced in the detection process as well as in the reconstruction process based on primitives extracted in the images.

In this paper, we proposed an automated road lane marking extraction approach based on multi-resolution image analysis and anisotropic Gauss filtering. The road centerline is firstly detected from the low resolution image, which provides the local orientation and rough location of the road surface. Anisotropic Gauss filtering is further employed to extract the road pavement markings on the

generated road surface. The workflow of our road lane marking extraction algorithm is as shown in Figure 1.

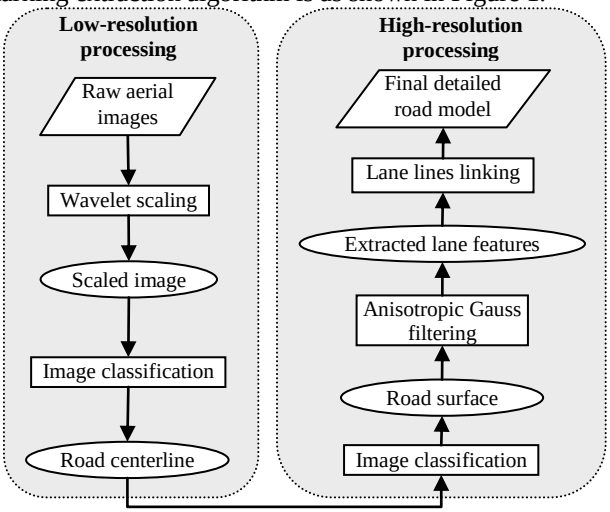

Figure 1. Flowchart of the proposed system for road marking extraction.

The reminder of this paper is organized as follows. In section 2, the original aerial image is decomposed to get the low resolution image using Discrete Wavelet transform. Road centerline is then extracted from the low resolution image using ISODATA algorithm. In section 3, road surface is extracted from the high resolution image using the generated road centerline, and road pavement markings are further detected with anisotropic Gauss filtering. System testing and quantitative evaluation is then given in section 4. Finally, the concluding remarks are presented in section 5.

II. ROAD CENTERLINE DETECTION

The basic function of multi-resolution image analysis approach is based on the fact that different characteristics of road features can be best detected in different scales. On one hand, road lane details can only be detected in high precise images, but at the same time, many local disturbances such as shadows can also greatly degrade the results. On the other hand, the road position can be easily extracted in lower resolution images, where roads are basically considered as homogeneous bands of different lengths and orientations. Therefore, it is beneficial to extract the desired road features at different resolution and consequently combine the individual level result to obtain the refined output.

We employ 2D Discrete Wavelet Transform (DWT) instead of pyramid analysis to obtain the low resolution image as it can maximally preserve the essential information content. In the decomposition of image via wavelet transform, proper choice of wavelet is an important issue. More than 4300 candidate filter banks were tested in [13], and the biorthogonal (9,7) pair has almost the best performance in maintaining good visible quality through the use of bit allocation in the sub-images. Therefore, the Bior(9-7) filter bank is utilized here. An example of image composition is shown in Figure 2, the original aerial image (Figure 2(a)), which has a resolution of 0.1 m and the size of 1024×1024, is decomposed four levels to a resolution of 0.8 m with the size of 64×64 (Figure 2(b)).

The first step of low level image analysis is image segmentation, the success of which is critical for the successfully detection of road centerlines. To ensure that only necessary features would involve in the separability of road surface, color space transformation is employed to select the appropriate image data. As the road surface made of asphalt appears as relatively white under the strong illumination of direct sun light in Queensland, which can be utilized to assist the color space selection.

a b

Figure 2. An example of image wavelet decomposition, (a) and (b) are the original and the decomposed aerial images, respectively.

It is necessary to ensure that no more features than necessary are utilized when performing clustering. The redundancy of the original image can be checked by examining the correlation matrix between the spectral bands. The correlation matrix of the image shown in Figure 2(b) is

$$\begin{bmatrix} 1.00 & 0.99 & 0.97 \\ 0.99 & 1.00 & 0.96 \\ 0.97 & 0.96 & 1.00 \end{bmatrix}$$

It is apparent that the *R*, *G*, and *B* bands within this image are highly correlated. Thus, the Principal Component Analysis (PCA) transform is utilized to reduce the number of image dimension while preserve the essential information content of the image. The eigen-values of the covariance in Figure 2(b) are $[4904.43 \quad 76.57 \quad 14.97]$, which means the 1st component account for 96.4% of the total information in the image. Therefore, only the 1st component of PCA transform is selected for further processing.

In HSI color space, the distance between the different RGB values determines the saturation component: the closer they are together, the lower the saturation. The road surface presents relatively white compared with other features, i.e. grasslands, which means it has low saturation component values. The conversion from RGB to HSI is defined as:

$$\begin{cases} H = \text{Arccos}\left(\dfrac{\frac{(\text{R}-\text{G})}{2}+(R-B)}{\sqrt{(R-G)^2+(R-B)(\text{G}-\text{B})}}\right) \\ S = 1 - \dfrac{\min(R,G,B)}{I} \\ I = \dfrac{R+G+B}{3} \end{cases} \quad (1)$$

- If $S = 0$, H is meaningless.
- If $(B/I) > (G/I)$ then $H = 360 - \text{H}$

As the vegetation areas, including bushes and grassland, have relatively low value of blue component in RGB, the C_b component in YC_rC_b color space is selected to distinguish the road surface from these vegetation lands. YC_rC_b is defined as:

$$\begin{bmatrix} Y \\ C_b \\ C_r \end{bmatrix} = \begin{bmatrix} 0.257 & 0.504 & 0.098 \\ -0.148 & -0.291 & 0.439 \\ 0.439 & -0.368 & -0.071 \end{bmatrix} \begin{bmatrix} R \\ G \\ B \end{bmatrix} + \begin{bmatrix} 16 \\ 128 \\ 128 \end{bmatrix} \quad (2)$$

where Y is the brightness, C_r is the red-difference $(R - Y)$, and C_b is the blue-difference $(B - Y)$.

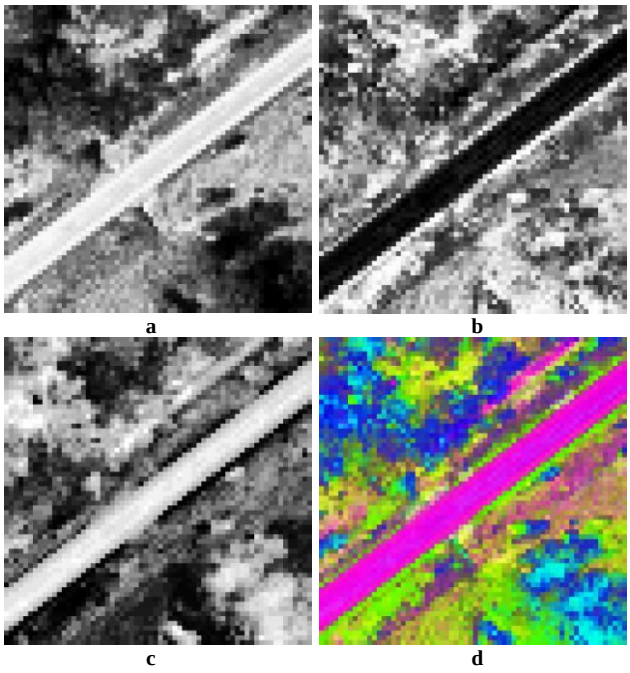

Figure 3. Three transferred color bands of image Figure 2(b), (a) 1st component of PCA transform, (b) the saturation band from HSI color space, (c) the C_b component from YC_rC_b color space, and (d) the composed result with the above three images.

The 1st component of PCA transform, the saturation band from HSI color space, and the C_b component in YC_rC_b color space are acquired and stretched using the histogram equalization algorithm to enhance their global contrast respectively. Then they are further fused using 1st component of PCA as *R* band, saturation component as *G* band, and C_b component as *B* band, the stretched three bands and the fused image is shown in Figure 3(d).

After the data preparation, the image segmentation approach can be used to classify road surface from other ground objects. The unsupervised ISODATA algorithm is used in our work to segment the aerial image. Three classes, which correspond to road regions, vegetations, and shadows, are determined (as shown in Figure 4(a)). Segments are selected as road features if the following two criteria are satisfied: (i) the mean width of the segment is within a certain range, (ii) the length to width ratio is larger than a preset threshold. Besides, the area filter method is utilized to remove small noises that are misclassified into road class. After the extraction of road surface, a modified Wang-Zhang thinning algorithm [14] is further employed to extract the skeletons form the road segment. The generated road centerline is actually zigzag thanks to the disturbances from shadows or variation of road width. Therefore, the least squares line approximation is an appropriate method to fit a linear relation between the extracted road centerline points, and the result is given in Figure 4 (b).

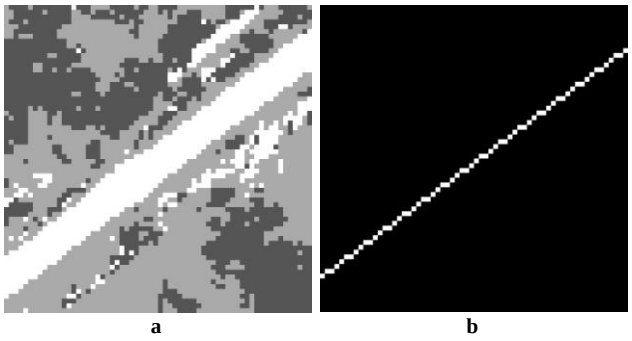

Figure 4. (a) the result of image segmentation (White: road regions, Grey: vegetation, and Black: shadows), and (b) the extracted road centerline, which was approximated by least squares line method.

III. Road Surface and Lane Marking Extraction

Up to now, we have obtained the road centreline from the low-resolution image. And thus the orientation and the rough position of the road surface within high-resolution image can be easily acquired. The orientation θ can be calculated using the two endpoints $P1(x_1, y_1)$ and $P2(x_2, y_2)$ of the centreline segment (See Figure 4.4), which can be derived by

$$\theta = \arctan\left(\frac{y_2 - y_1}{x_2 - x_1}\right)$$

Since the vegetation regions have relatively low value of C_b component in YC_rC_b colour space, only the C_b component is utilized to extract the road surface in the original image.

The contrast enhanced C_b component of the original aerial image is as illustrated in Figure 5(a). As one of the widely used techniques for monochrome image segmentation, histogram thresholding is utilized here to segment the aerial image. The Otsu's algorithm [16] is applied on the histogram to automatically determine the threshold. The Otsu's method finds the optimal threshold *T*, which maximizes

$$V(T) = \frac{\left(\bar{\mu} \cdot \omega(T) - \mu(T)\right)^2}{\omega(T) \cdot \mu(T)} \quad (3)$$

where $\omega(T) = \sum_{i=0}^{T} p_i$, $\mu(T) = \sum_{i=T+1}^{255} p_i$, $\bar{\mu} = \sum_{i=0}^{255} i \cdot p_i$, p_i is the probability of pixels with grey level i in the image. Two classes, which correspond to road regions, vegetation areas are determined. We can see that the road surface has been perfectly segmented as white object in the image. Segments are selected as road features if the following two criteria are satisfied: (i) the mean width of the segment is within a certain range, (ii) the length to width ratio is larger than a preset threshold. Besides, the area filter method is utilized to remove small noises that are misclassified into road class. The two sides of the segmentation result are

further smoothed by the least squares line approximation, and the final road surface is given in Figure 5(d).

A fast anisotropic Gaussian filter was been proposed by GeuseBroek and Smeulders [16] in 2003. The orientation filter in two dimensions is given by the convolution of two Gaussian filters, presented as:

$$G(u,v) = \frac{1}{\sqrt{2\pi}\sigma_u\sigma_v}\exp[-\left(\frac{u^2}{2\sigma_u^2}+\frac{v^2}{2\sigma_v^2}\right)] \quad (4)$$

where $u = x\cos\theta + y\sin\theta$ and $v = -x\sin\theta + y\cos\theta$.

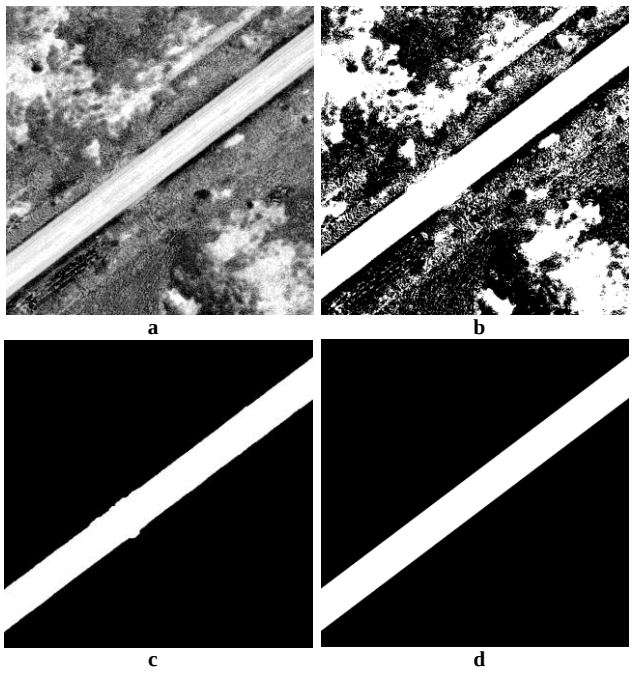

Figure 5. Image unsupervised segmentation, (a) enhanced C_b component image, (b) image segmentation result, (c) extracted road surface class, and (d) road sides smoothed by least square line approximation

θ is the orientation of the anisotropic Gaussian filter, x and y are the Cartesian coordinates of the image pixels. Anisotropic Gauss filter can be considered as orientation and scale tunable edge and line (bar) detector, which makes it a perfect method for the detection of geometrical restricted linear features, such as the road lane markings.

The correct determination of anisotropic Gauss filter parameters is the central issue for the lane pavement marking extraction. The parameter θ is set to the rough direction of the road centerline, which is already obtained from the low resolution image. The ratio of σ_u and σ_v is set to 2 based on the road pavement marking guide [17], as the least length to width ratio of the lane marking is 2. σ_v is determined by the half width of the pavement marking, as the average width of pavement marking in the image of Figure 2(a) is 3 pixels, thus σ_v is set to be 1.5 here.

Anisotropic Gauss filtering is utilized to extract the lane marking features while restrain the affection from other ground objects. To reduce the calculation complexity, PCA method is applied on the RGB image and only the 1st component is chosen for Gauss filtering. The orientation of the markings is obtained by the centerline in the low resolution image, which is 36.87 degrees for the example image. The filtered image is given in Figure 6(b), which is then masked by the road surface acquired in the previous step.

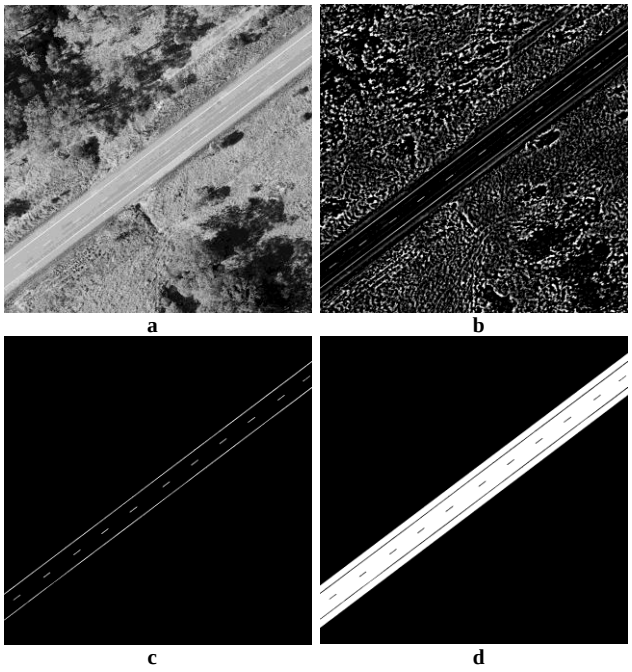

Figure 6. Road lane marking detection, (a) 1st component of PCA tranform of the original image, (b) anisotropic Gauss filter image, (c) extracted road marking, and (d) generated pavement markings superimposed on the extracted road surface.

In the filtered image, the pavement markings with white or grey color had a much higher brightness value than the road pavement areas composed of dark asphalt. The geometric properties and spatial relationships can be further utilized for the selection of lane marking candidates:

- The geometric properties of the lane markings were calculated: the lengths, widths, directions, together with the areas were examined by the road construction manuals [17]. Only regions satisfying the rules specified in the manual were selected as suitable candidates.
- The distance and orientation difference between neighboring lane markings candidates were calculated and analyzed. Only the candidates with similar orientation and particular distances would be preserved for further processing.

The final extracted road lane marks are displayed in Figure 6(c), and Figure 6(d) shows the generated road marks superimposed on the extracted road surface.

IV. Experiemnts and Evaluatoin

A set of high-resolution aerial panchromatic images taken on 28 November 2008 using the UltraCam-D digital camera was used as the test data set. The image scale is 1:11081, and pixel size is 9μm (about 10 cm ground spatial resolution). The test sites were parts of the Bruce highway, located in Gympie, Queensland. The testing road is a single carriageway with 2 lanes in the majority of road segments.

In order to evaluate the results, we compare the obtained road lane feature to a manually digitized reference road dataset. The road marking accuracy evaluation is carried out by comparing the extracted pavement marks with manually plotted markings used as reference data as presented in [18], and both data sets are given in vector representation. The buffer width is predefined to be the average width of the road markings, and we set it to be 15 cm in our experiment. Then the accuracy measures are given as:

1) Detection rate

$$d = \frac{\text{length of the matched reference}}{\text{length of reference}}$$

2) False alarm rate

$$f = \frac{\text{length of the unmatched extraction}}{\text{length of extraction}}$$

3) Quality

$$q = \frac{\text{length of the matched reference}}{\text{length of extraction} + \text{unmatched reference}}$$

We selected 8 testing areas from the dataset, which covers an area of approximate 2 km^2. The average detection rate is about 97.8%, false alarm rate is only 2.9%, and quality reaches 94.6%. The success of lane feature detection largely depends on the assumption that the road surface and pavement markings are straight within the processing image, thus it only works well when the lane marking within the image is approximately linear. Therefore, the processing image has to be restricted within a limited area to keep the road straight. As to the process of large images, image partition method can be utilized so that large image can be divided into smaller sub-images before the road feature extraction.

V. CONLUDING REMAKRS

In this paper, a novel road surface and pavement marking extraction approach from high resolution aerial images is proposed. The developed method, which is based on multi-resolution image analysis as well as anisotropic Gauss filtering, can generate accurate lane level digital road maps automatically. The experimental results using the stereo digital aerial image dataset with ground resolution of 0.1 m have demonstrated that the proposed method works satisfactorily. Further work will concentrate on the process of seriously curved road surface and large images, which may be achieved by using knowledge based image analysis and image partition technique.

ACKNOWLEDGMENT

This work is partially supported by Chinese Scholarship Council (Grant No: 2007101585). The testing aerial image dataset is kindly provided by the Department of Transport and Mains Roads, Queensland.

REFERENCES

[1] H. Gontran, J. Skaloud, and N. Janvier, "Open-source software-operated CMOS camera for real-time mapping," in the International Archives of the Photogrammetry, Remote Sensing and Spatial Information Sciences, Paris, France, 2006.

[2] C. Kreucher and S. Lakshmanan, "LANA: a lane extraction algorithm that uses frequency domainfeatures," IEEE Transactions on Robotics and Automation, vol. 15, pp. 343-350, 1999.

[3] A. H. S. Lai and N. H. C. Yung, "Lane detection by orientation and length discrimination," IEEE Transactions on Systems, Man, and Cybernetics Part B: Cybernetics, vol. 30, pp. 539-548, 2000.

[4] Y. Wang, E. K. Teoh, and D. Shen, "Lane detection and tracking using B-Snake," Image and Vision Computing, vol. 22, pp. 269-280, 2004.

[5] P. Jeong and S. Nedevschi, "Efficient and robust classification method using combined feature vector for lane detection," IEEE Transactions on Circuits and Systems for Video Technology, vol. 15, pp. 528- 537, 2005.

[6] B. Soheilian, "Roadmark reconstruction from stereo-images acquired by a ground-based mobile mapping system," in Sciences de l'Information Géographique Marne-la-Vallée, France: Université Paris-Est 2008.

[7] C. Steger, H. Mayer, and B. Radig, "The role of grouping for road extraction," in Automatic Extraction of Man-Made Objects from Aerial and Space Images (II). vol. 245-256, 1997, pp. 1931-1952.

[8] S. Hinz and A. Baumgartner, "Automatic extraction of urban road networks from multi-view aerial imagery," ISPRS Journal of Photogrammetry and Remote Sensing, vol. 58, pp. 83-98, 2003.

[9] C. Zhang, "Towards an operational system for automated updating of road databases by integration of imagery and geodata," ISPRS Journal of Photogrammetry and Remote Sensing, vol. 58, pp. 166-186, 2004.

[10] R. Rushone and S. Airault, "Toward an automatic extraction of road network by local interpretation of the scene," Photogrammetric Week, pp. 147-157, 1997.

[11] O. Tournaire and N. Paparoditis, "A geometric stochastic approach based on marked point processes for road mark detection from high resolution aerial images," ISPRS Journal of Photogrammetry and Remote Sensing, vol. 64, pp. 621-631, 2009.

[12] J. G. Kim, D. Y. Han, K. Y. Yu, Y. I. Kim, and S. M. Rhee, "Efficient extraction of road information for car navigation applications using road pavement markings obtained from aerial images," Canadian Journal of Civil Engineering, vol. 33, pp. 1320-1331, 2006.

[13] J. D. Villlasenor, B. Belzer, and J. Liao, "Wavelet filter evaluation for image compression," IEEE Transactions on Image Processing, vol. 4, pp. 1053-1060, 1995.

[14] P. S. P. Wang and Y. Y. Zhang, "A fast and flexible thinning algorithm," IEEE Transactions on Computers, vol. 38, pp. 741-745, May 1989.

[15] N. Otsu, "A threshold selection method from gray level histograms," IEEE Transactions on Systems, Man and Cybernetics, vol. 9, pp. 62-66, 1979.

[16] J.-M. Geusebroek, A. W. M. Smeulders, and J. v. d. Weijer, "Fast anisotropic Gauss filtering," IEEE Transactions on Image Processing, vol. 12, pp. 938-943, 2003.

[17] Queensland Department of Main Roads, Guide to pavement markings, 2 ed. Brisbane, Queensland: Department of Main Road, 2001.

[18] C. Wiedemann, C. Heipke, H. Mayer, and O. Jamet, "Empirical evaluation of automatically extracted road axes," in *Empirical Evaluation Methods in Computer Vision*, J. B. Kevin and P. J. Phillips, Eds.: IEEE Computer Society Press, 1998, pp. 172-187.